

H₂ production through electro-oxidation of SO₂: identifying the fundamental limitations†

Cite this: *Phys. Chem. Chem. Phys.*, 2014, 16, 9572

Roelof J. Kriek,^{*a} Jan Rossmeisl,^b Samira Siahrostami^b and Mårten E. Björketun^{*b}

Sulphur dioxide (SO₂), a known industrial pollutant and pulmonary irritant, is emitted to the atmosphere in excess of 120 Mt per annum. Great strides have been taken to reduce SO₂ emissions, but with the growth of specifically China, and to a lesser extent India, it is on the rise again. The electrolysis of aqueous solutions of dissolved SO₂ holds huge environmental potential in that SO₂ is converted to sulphuric acid (H₂SO₄) and at the same time hydrogen gas is produced. A further benefit or incentive is that a sulphur depolarised electrolyser (SDE) operates at an applied potential that is about one volt lower than that of a regular water electrolyser. In taking this technology forward the greatest improvement to be made is in developing a suitable electrocatalyst, which is also the 'lowest hanging fruit' in that very limited research and development has been conducted on the electrocatalyst for this process. In this work, density functional theory is employed to model the electro-oxidation of SO₂ on single crystal planes of the 4d and 5d transition metals. Two reaction mechanisms are considered, a HSO₃ intermediate pathway and a SO₃ intermediate pathway. The binding energies of all intermediates are found to scale with the surface reactivity (measured as the adsorption of OH). Irrespective of the pathway water needs to be activated and reduction of SO₂ to elemental sulphur must be avoided. This requirement alone calls for an electrode potential of at least 0.7–0.8 V for all the investigated transition metals and thus challenges the proclaimed goal to operate the SDE at 0.6 V. A high chemical barrier is further found to severely limit the oxidation reaction on reactive metals. A much higher catalytic activity can be obtained on precious metals but at the cost of running the reaction at high overpotentials.

Received 17th February 2014,
Accepted 1st April 2014

DOI: 10.1039/c4cp00705k

www.rsc.org/pccp

1. Introduction

Industrialisation, economic growth and global population increase have resulted in an increasing demand for energy, which has inevitably been coupled to an increasing release of pollutants in that fossil fuels (coal, petroleum and natural gas) have predominantly been used as energy sources. In turn the global scientific community has been spurred on, during the last few decades, to research and develop clean(er) processes. If energy supply is not green (non-polluting and sustainable) from the outset, such as wind and solar, it is inevitable that those processes would go hand in hand with the release of environmental pollutants. One such pollutant is sulphur dioxide (SO₂) that results from coal fired power stations, oil refining and other industrial processes. Around the mid 1970s global sulphur

dioxide (SO₂) emissions peaked after which it started to decline, but with the growth of specifically China, and to a lesser extent India, SO₂ emissions are on the rise again (Fig. 1).¹ The reduction in SO₂ emissions, specifically in Europe and North America, is attributed to the implementation of dedicated abatement technologies and to a lesser extent as a result of the implementation

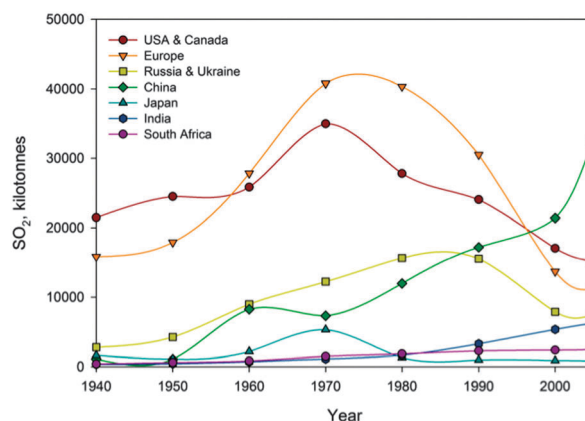


Fig. 1 Anthropogenic SO₂ emissions for specific countries and regions as of 1940.

^a PGM Group, Research Focus Area for Chemical Resource Beneficiation (CRB), North-West University, Potchefstroom 2520, South Africa.
E-mail: cobus.kriek@nwu.ac.za; Tel: +27 (0)18 299 2345

^b Center for Atomic-scale Materials Design (CAMD), Department of Physics, Technical University of Denmark, DK-2800 Lyngby, Denmark.
E-mail: martebjo@fysik.dtu.dk

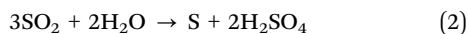
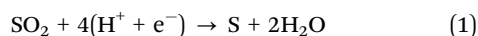
† Electronic supplementary information (ESI) available: Kinetic modelling. See DOI: 10.1039/c4cp00705k

of cleaner processes. Global anthropogenic SO₂ emissions totalled 127 Mt in 2008, with energy production totalling 63.2 Mt (2008) and metal related processes totalling 12.8 Mt (2008).² From a health perspective it is well-known that SO₂ acts as a pulmonary irritant and to that regard it affects the nose, throat and lungs, as well as the eyes and skin. From an environmental perspective SO₂ emissions result in acid rain that impacts negatively on both the built- and natural environment.

The research and development of clean(er) energy processes has, amongst others, focussed substantially on water electrolysis as a means of producing hydrogen (a clean energy carrier). To that regard the oxygen evolution reaction has been the focus of numerous investigations with a few review papers having been published.^{3,4} Water is oxidised at the anode of a proton exchange membrane (PEM) electrolyser and the produced protons (hydrogen ions) migrate through the membrane and are reduced at the cathode to hydrogen gas, the net result being the splitting of water into oxygen and hydrogen, according to Table 1(a). By adding SO₂ to the anode of the electrolyser the anodic standard equilibrium potential comes down from 1.23 V *versus* the reversible hydrogen electrode (RHE), for regular water electrolysis, to 0.16 V (RHE), for SO₂ water electrolysis (Table 1(b)), which equates to an energy saving of more than one volt.

During this process hydrogen ions are still produced, but in the process a serious environmental pollutant is converted to a more manageable compound, *i.e.* sulphuric acid.

Although SO₂ water electrolysis owes its 'birth' to the Westinghouse process or the Hybrid Sulphur (HyS) cycle,⁵ a combination of a thermal process decomposing sulphuric acid into sulphur dioxide and oxygen and an electrochemical process to electro-oxidise aqueous SO₂ to produce hydrogen and sulphuric acid and thereby closing the cycle, there would now seem to be a drive to focus only on the sulphur depolarised electrolyser (SDE) as a means of developing an 'energy producing abatement technology' as indications are pointing towards the net production of energy if a power plant's waste heat is to be coupled to this process.⁶ With the SDE operating at an aimed current density of 500 mA cm⁻² and an aimed cell potential of 0.6 V,⁷ at around 100 °C, elemental sulphur is bound to deposit on the anode of the SDE according to both an electrochemical reaction (reaction (1))⁸ and a disproportionation reaction (reaction (2)).⁹



Electrocatalysts for the oxygen evolution reaction, the anodic reaction in acid electrolysers, have been studied extensively, both theoretically^{10,11} and experimentally.¹²⁻¹⁹ In comparison electrocatalysts for SO₂ water electrolysis have been afforded

very limited investigation and, other than a single paper by Lee and Langer²⁰ on Pt/Al bimetallic catalysts, only the pure noble metals, platinum and palladium,²¹⁻²⁵ as well as gold,²⁶⁻²⁸ have to some extent been investigated for this reaction. Lee and Langer²⁰ found that the doping of platinum with a small amount of aluminum (Al), in a bimetallic form (not alloyed), exhibited a large improvement in electrode performance. The goal of running the SDE at a cell potential of 0.6 V and a current density of 500 mA cm⁻² has, however, not been reached. Attaining this goal will only be possible if a concerted effort is made to develop a suitable electrocatalyst that is able to sufficiently reduce the overpotential on the anode of the SDE.

We herein report on the first density functional theory (DFT) investigation to elucidate the activity of the transition metals – specifically the 4d transition metals Nb, Mo, Ru, Rh, Pd and Ag, and the 5d transition metals Ta, W, Os, Ir, Pt and Au – for the electro-oxidation of sulphur dioxide in aqueous medium. Different reaction mechanisms of the electro-oxidation of SO₂ in aqueous solutions have been suggested. It has been reported that OH formation could be the first step in the mechanism,^{24,29} while others suggest that sulphate²¹ or bisulphate²⁶ is formed during the first step, with a further suggestion that the dithionate ion^{30,31} is in fact the first intermediate. Our point of departure, however, is that ideally a catalyst is required that (i) does not favour the reduction of SO₂ to elemental sulphur (S), thus preventing poisoning of the catalyst, and (ii) is able to activate water. To that regard we are considering two potential reaction paths with the first reaction step geared towards preventing the reduction of SO₂ to elemental sulphur (S) followed by two different water splitting reactions (Table 2), *i.e.* over (Path 1) a bisulphite (HSO₃) intermediate, and (Path 2) a sulphite (SO₃) intermediate.

2. Results and discussion

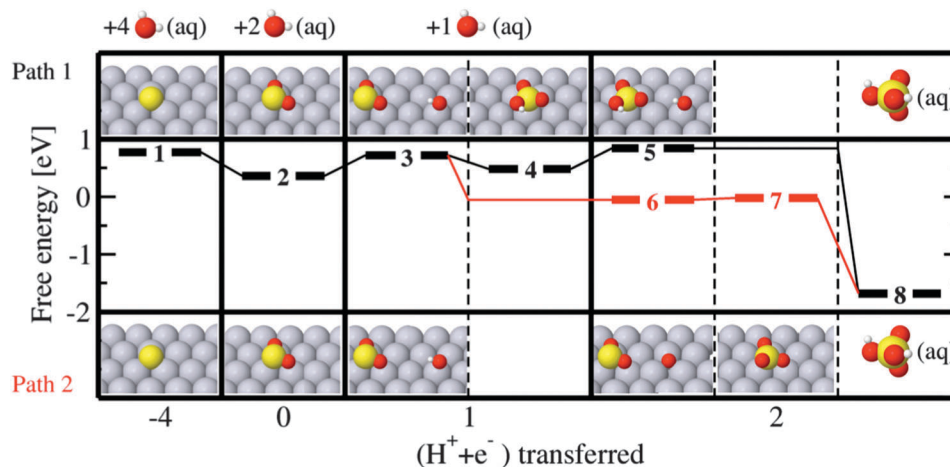
Fig. 2 depicts SO₂ electro-oxidation over Pt(111) along the two competing paths (Path 1 and Path 2) proposed in Table 2. The figure reports the most stable adsorption geometries for the various intermediates – S*, SO₂*, OH*, HSO₃*, O* and SO₃* (* denotes a site on the surface that the intermediate attaches to) – together with the corresponding reaction free energy diagram at *U* = 1 V *vs.* RHE. More precisely, S and O adsorb in 3-fold fcc sites; OH* occupies on-top sites in an almost flat-lying position; SO₂* is planar and centred over an fcc site with the three atoms each coordinating to a different surface Pt; SO₃ adsorbs in a bridge-type position with S coordinating to one Pt, one of the Os coordinating to a neighbouring Pt and the remaining two Os pointing away from the surface; and, finally, HSO₃ adsorbs atop, with S coordinating to Pt and the remaining atoms pointing away from the surface. The reaction diagram contains a combination of

Table 1 (a) Regular water electrolysis vs. (b) SO₂ electrolysis

(a)	<i>E</i> ⁰ /V (RHE)	(b)	<i>E</i> ⁰ /V (RHE)
2H ₂ O → O ₂ + 4(H ⁺ + e ⁻)	1.23	SO ₂ + 2H ₂ O → H ₂ SO ₄ + 2(H ⁺ + e ⁻)	0.16
4(H ⁺ + e ⁻) → 2H ₂		2(H ⁺ + e ⁻) → H ₂	
2H ₂ O → O ₂ + 2H ₂ (net reaction)		SO ₂ + 2H ₂ O → H ₂ SO ₄ + H ₂ (net reaction)	

Table 2 Reaction paths for aqueous SO₂ electro-oxidation following the HSO₃ intermediate path (Path 1), and the SO₃ intermediate path (Path 2)

(Path 1)	(Path 2)
$S^* + 2H_2O \rightarrow SO_2^* + 4(H^+ + e^-)$	$S^* + 2H_2O \rightarrow SO_2^* + 4(H^+ + e^-)$
$* + H_2O \rightarrow OH^* + (H^+ + e^-)$	$* + H_2O \rightarrow OH^* + (H^+ + e^-)$
$SO_2^* + OH^* \rightarrow HSO_3^* + *$	$OH^* \rightarrow O^* + (H^+ + e^-)$
$* + H_2O \rightarrow OH^* + (H^+ + e^-)$	$SO_2^* + O^* \rightarrow SO_3^* + *$
$HSO_3^* + OH^* \rightarrow H_2SO_4 + 2*$	$SO_3^* + H_2O \rightarrow H_2SO_4 + *$
$S^* + 4H_2O \rightarrow H_2SO_4 + 6(H^+ + e^-) + *$ (net reaction)	$S^* + 4H_2O \rightarrow H_2SO_4 + 6(H^+ + e^-) + *$ (net reaction)

**Fig. 2** Free energy diagram for oxidation of SO₂ to H₂SO₄ and reduction of SO₂ to S over Pt(111) at $U = 1$ V vs. RHE. Two competing oxidation pathways are investigated: Path 1 (top cartoons, black energy levels) and Path 2 (bottom cartoons, black/red energy levels). The bottom axis indicates the total number of proton–electron pairs that have been transferred at each intermediate state along the reaction path. The top bar shows the number of water molecules that must be added to individual states in order to preserve the stoichiometry of the reaction.

electrochemical and chemical steps; the potential dependent electrochemical steps, involving transfer of one or several proton–electron pairs, connect intermediates separated by solid vertical lines, whereas the potential independent chemical steps cross dashed vertical lines. The free energy of intermediates X^* have been calculated relative to SO₂(g), H₂O(l), and proton–electron pairs H⁺(aq) + e⁻, assuming standard conditions.

They are thus reaction free energies and can be expressed as $\Delta G_{X^*} = \Delta G_{X^*}^0 - neU$, where n is the number of transferred H⁺(aq) + e⁻ pairs, U the potential vs. RHE, and $\Delta G_{X^*}^0$ the adsorption free energy at $U = 0$ V vs. RHE. If one of the cartoons contains two adsorbates, X^* and Y^* , the corresponding free energy is given by $\Delta G_{X^*+Y^*} = \Delta G_{X^*}^0 + \Delta G_{Y^*}^0 - neU$. Accordingly, once all $\Delta G_{X^*}^0$ have been calculated the free energy diagram can be drawn at any potential of interest (the equations used to calculate the different $\Delta G_{X^*}^0$ are reported in Section 4). The figure would look similar for other metals, but the adsorption geometries could differ and the free energies of the adsorbates would most certainly be different. We used Pt(111) merely as an illustration as it is the single crystal transition metal catalyst most commonly used for SO₂ electro-oxidation, and as it turns out also one of the most efficient.

We have calculated $\Delta G_{X^*}^0$ of the intermediates along Path 1 and Path 2 on the close-packed surfaces of all the considered 4d and 5d transition metals. Fig. 3 shows the $\Delta G_{X^*}^0$ plotted against

$\Delta G_{OH^*}^0$ on the different metal surfaces. It is evident that, except for a few outliers, the adsorption energies scale linearly with the reactivity of the surface³² (here measured as the adsorption of OH) and that the binding decreases from left to right along the rows in the periodic table. In the discussion that follows these scaling relations will be used to gain a general understanding of the electrochemical performance of transition metals toward electro-oxidation of SO₂. Individual data points, on the other hand, will be used to disclose the electrochemistry on specific metals.

We start by noting that the binding energies of elemental sulphur are substantially greater (by about 2 eV) than those of any of the other reaction components. This would seem to be in line with experimental observations that elemental sulphur is easily deposited, *i.e.* SO₂ is reduced to S, on the working electrode of a three-electrode cell as a result of different preconditioning procedures.^{8,27,28,33}

The strong sulphur binding affects the oxidation negatively; in order to generate any appreciable amount of the desired products, H₂ and H₂SO₄, the reaction paths depicted in Fig. 2 have to be downhill in free energy, and to sufficiently destabilize sulphur relative to other reaction components for this to happen requires a considerable bias potential. Without possessing detailed knowledge about the actual reaction mechanism one can also conclude that successful production of H₂ and

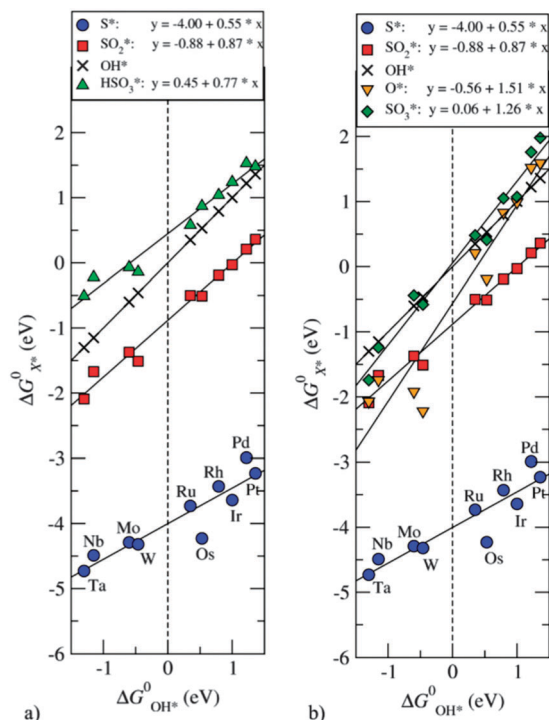


Fig. 3 Scaling between the adsorption energies of the intermediates in (a) Path 1 and (b) Path 2 at $U = 0$ V vs. RHE.

H_2SO_4 is contingent on activation of $H_2O(l)$ (*i.e.* OH^* should be adsorbed). Oxidation of S^* to SO_2 , and subsequent adsorption of OH^* , occurs according to reaction (3) and therefore requires transfer of 5 proton–electron pairs.



Since the binding of S^* and OH^* scales, there is a lower limit to the potential needed to activate the process. We obtain this potential by subtracting $\Delta G_{S^*}^0$ from $\Delta G_{OH^*}^0$ and dividing by 5 electrons, see Fig. 4. The average potential needed is ~ 0.8 V, corresponding to an overpotential of at least 0.65 V for SO_2 electro-oxidation on most elemental transition metal catalysts. The onset potential is slightly lower on the more reactive metals. This would suggest that they might be the most promising catalysts, but as we will see later another limiting mechanism makes them less viable. This simple consideration shows that the proposed 0.6 V target will be difficult to reach using catalysts obeying the current scaling relation between S^* and OH^* .

Next, we compare the two proposed reaction pathways, Path 1 and Path 2. Path 1 goes through a state consisting of HSO_3 and OH co-adsorbed on the surface while Path 2 goes through a state with co-adsorbed SO_2 and O . An identical number of proton–electron pairs have been transferred in the two states so the two energy levels will respond identically to a change in potential. Hence, it is sufficient to compare $\Delta G_{X^*}^0 + \Delta G_{Y^*}^0$ of the two states in order to predict the path preference at any potential.

Fig. 5 reports the energy difference as a function of $\Delta G_{OH^*}^0$, with squares indicating the results for individual metals and

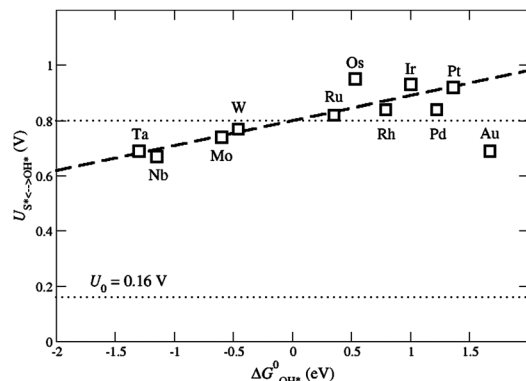


Fig. 4 Potential required to favour OH^* adsorption compared to S^* adsorption.

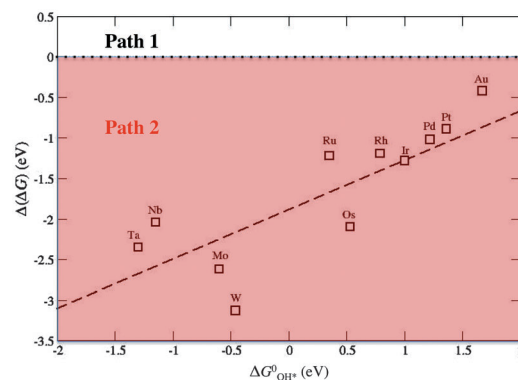


Fig. 5 Difference between $\Delta G_{SO_2^*}^0 + \Delta G_{O^*}^0$ and $\Delta G_{HSO_3^*}^0 + \Delta G_{OH^*}^0$. The dashed line represents the free energy difference, $\Delta(\Delta G)$, as given by the linear correlations in Fig. 3 and the squares indicate the corresponding differences calculated for individual atoms. $\Delta(\Delta G)$ is potential independent and negative for all but extremely inert materials, meaning that Path 2 will dominate.

the dashed line showing the general trend as given by the scaling relations in Fig. 3. Our calculations predict that Path 2 will dominate on all potentially interesting metals. From now on we will thus focus on Path 2 and investigate the thermochemistry and kinetics of that reaction path in some detail. In reality, the two pathways may compete on the most noble metals since the solvent (water), which has not been included in the present calculations, tends to stabilize OH^* with respect to O^* .³⁴ However, as shown in the ESI,[†] the general conclusions would be almost identical if we instead chose to study Path 1.

In Fig. 6 we have plotted the reaction free energies, $\Delta G_{\alpha \rightarrow \beta}$, of the elementary steps in Path 2 against $\Delta G_{OH^*}^0$ at four potentials, $U = 0.6, 0.8, 1.0$ and 1.2 V vs. RHE. At $U = 0.6$ V the more reactive metals ($\Delta G_{OH^*}^0 \leq 0.5$ eV) are limited by the chemical step, $6 \rightarrow 7$, while the other metals are limited by the first electrochemical step, $1 \rightarrow 2$. (See Section 4 and the ESI[†] for all reaction steps.) On highly inert materials ($\Delta G_{OH^*}^0 \geq 1.9$ eV), activation of water, $2 \rightarrow 3$, would be limiting. At this potential the catalytically most active materials have a $\Delta G_{OH^*}^0$ of approximately 0.5 eV. However, even on the most active metals the

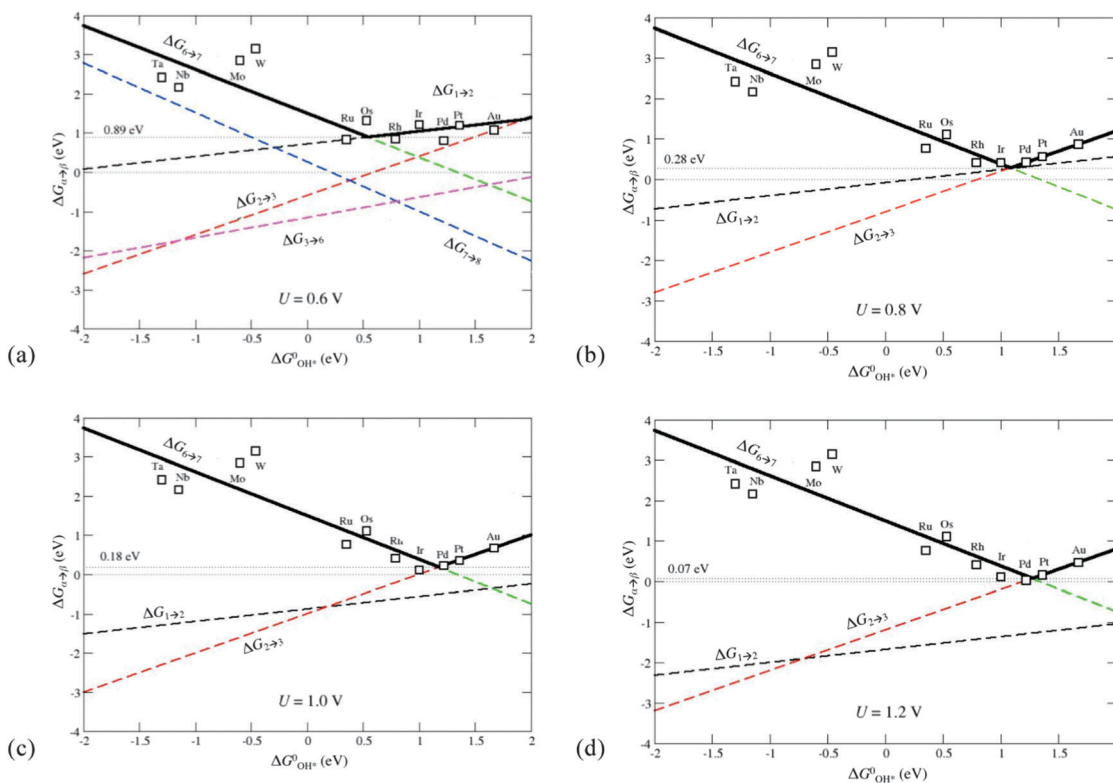


Fig. 6 Reaction free energy of the elementary steps along Path 2 as a function of $\Delta G_{\text{OH}^*}^0$ at (a) $U = 0.6$ V, (b) $U = 0.8$ V, (c) $U = 1.0$ V and (d) $U = 1.2$ V on the RHE scale. The free energy of the limiting step(s) is indicated with a solid black line. Dashed lines are reaction free energies estimated from the linear correlations in Fig. 3, whereas squares indicate the maximum reaction free energy encountered along the reaction path for individual metals. The chemical step 7 \rightarrow 8 is excluded from plots (b)–(d) since it is always considerably more facile than the chemical step 6 \rightarrow 7. Likewise, the electrochemical step 3 \rightarrow 6 is excluded from all plots except (a) since its reaction free energy changes with potential as 2 \rightarrow 3 and it is lower in all cases of interest.

limiting reaction energy is high, of the order 0.9 eV, so the oxidation rate will be very low. The reactive materials, which are limited by 6 \rightarrow 7, have reached their maximum oxidation activity already at a lower potential since the chemical step does not change with potential.

Furthermore, the fact that $\Delta G_{1 \rightarrow 2}$ is positive on all considered metals at the current potential suggests that much of the SO_2 adsorbing on the surface will be reduced to S^* , which will block catalytically active sites and inhibit the oxidation reaction. When the potential is raised, the electrochemical barriers decrease and the oxidation runs faster over the less reactive metals. At $U = 0.8$ V virtually no metals are limited by step 1 \rightarrow 2. Instead, metals with $\Delta G_{\text{OH}^*}^0 \leq 1.0$ eV are limited by 6 \rightarrow 7 and the less reactive metals are limited by 2 \rightarrow 3. The most active materials are now found at $\Delta G_{\text{OH}^*}^0 = 1.0$ eV and the reaction free energy of their limiting step has been reduced to approximately 0.3 eV, which leads to a significantly enhanced oxidation current. When the electrode potential is raised further, 6 \rightarrow 7 and 2 \rightarrow 3 continue being the limiting steps, but the intersection of the two free energy lines is pushed to larger $\Delta G_{\text{OH}^*}^0$ and the maximum achievable activity becomes even higher (at 1.0 V the most active metal has a limiting reaction free energy of 0.18 eV and at 1.2 V it is reduced to 0.07 eV). On the most noble metals, where 6 \rightarrow 7 is

spontaneous, 2 \rightarrow 3 is the last step to become exergonic. These metals' peak potentials (the potential at which the maximum oxidation rate is first reached) are therefore expected to approximately coincide with the potential for OH adsorption, which can be deduced from cyclic voltammograms.

The above analysis shows that a high chemical barrier, which cannot be altered by electrode potential, will disqualify reactive metals as SO_2 electro-oxidation catalysts despite the facile oxidation of S^* to SO_2^* and adsorption of OH^* . A much higher activity can be obtained on less reactive metals but at the cost of running the reaction at high overpotentials. According to the graphs a metal with OH^* binding similar to that of Pt will be the best candidate; Pt is one of the least noble metals on which each elementary step along Path 2 can be made exergonic. This behaviour appears to be rather universal in electrocatalysis. On reactive metals the electrocatalysis is limited by high chemical barriers, essentially insurmountable at room temperature. On noble metals the chemical barriers are generally small, but the “electrochemical” protonation of reaction intermediates or activation of water requires a lot of energy input, which results in high overpotentials. Normally a metal with intermediate reactivity (often Pt) turns out to be the best compromise.

The above observations can be visualized in a comprehensible way by constructing a simple kinetic model, expression (4), of the SO₂ electro-oxidation along Path 2:

$$j_{\max}(U) \propto \nu \cdot \exp\left(-\max\left\{0, \min_{\Delta G_{\text{OH}^*}^0} \left\{\max_{\{\alpha, \beta\}} \Delta G_{\alpha \rightarrow \beta}(\Delta G_{\text{OH}^*}^0, U)\right\}\right\} / k_{\text{B}} T\right) \quad (4)$$

Expression (4) takes as input the $\Delta G_{\text{OH}^*}^0$ - and U -dependent reaction energies $\Delta G_{\alpha \rightarrow \beta}$ (the electrochemical steps are U -dependent, the chemical steps are not), calculated using the linear correlations in Fig. 3, and gives as output the maximum achievable oxidation current on any close-packed elemental transition metal surface at a given potential U . We are only interested in the relative activities of different materials, so we arbitrarily set the prefactor ν equal to 1. Furthermore, as before, we have ignored any additional barriers on top of the reaction energy. The calculated activity can therefore be viewed as an upper bound. Finally, the model ignores coverage effects, which

would influence absolute numbers but should have a smaller effect on predicted trends and general conclusions.

In Fig. 7 we have plotted the maximum oxidation rate, estimated by the model, against U (solid line). Additionally, Fig. 7 reports the maximum activity and the peak potential, U_{peak} , for the investigated close-packed transition metal surfaces. These activities have also been derived using the linear correlations, and that is the reason why they fall exactly on the solid line. It is important to note that this model is unable to predict drops in activity at higher potentials caused by oxidation of the surface. Fig. 7 suggests that the activity can be steadily increased for potentials up to ~ 1.35 V vs. RHE by employing increasingly noble catalysts. Beyond 1.35 V the activity saturates and there is nothing to gain in terms of current by using more noble catalysts.

In agreement with what we observed earlier, the kinetic model also shows that reactive metals are poor catalysts but reach their maximum activity at low potentials. If the stabilization of OH* by water is taken into account, the peak potential of the most noble metals (those with $U_{\text{peak}} \geq 1.35$ V) will be lowered with ~ 0.45 V (see the ESI† for details), a significant shift that would bring the peak potentials much closer to experimental values,⁸ but still far from the target potential. The reactive metals, on the other hand, will not be influenced by this effect.

3. Conclusions

To summarize, we have identified a set of physical/chemical relations that control the catalytic activity of transition metals toward electro-oxidation of SO₂. These constraints severely limit the number of metals that can be employed. In order for a metal to perform well a couple of criteria should be fulfilled. First of all, the metal surface should not be poisoned by atomic sulphur, *i.e.* reduction of SO₂ should be avoided, and water should be activated, *i.e.* OH should adsorb on the surface. This demand calls for a potential of at least 0.7–0.8 V for all the investigated transition metals. Secondly, the barrier of the chemical step encountered along the reaction pathway should be small, a requirement that effectively excludes all reactive metals. Thirdly, oxidation and dissolution of the surface must be avoided. This means that the electrode potential should be kept as low as possible, preferably below 1 V. We have seen that few elemental metals meet all these requirements; only Pt and a few other precious metals with similar OH binding exhibit decent catalytic performance.

Although it might be possible, through systematic screening,^{35,36} to identify an elemental or a binary metal catalyst that is cheaper and has similar or slightly better catalytic properties than Pt, great strides toward lower operating potentials and hence more efficient SEDs will require markedly different catalyst materials. Simply put, what a good catalyst must be able to do, which the elemental transition metals fail to do, is to promote the oxidation of SO₂ while inhibiting the reduction. One could imagine various ways of achieving this. One possibility could be to switch to another class of materials with

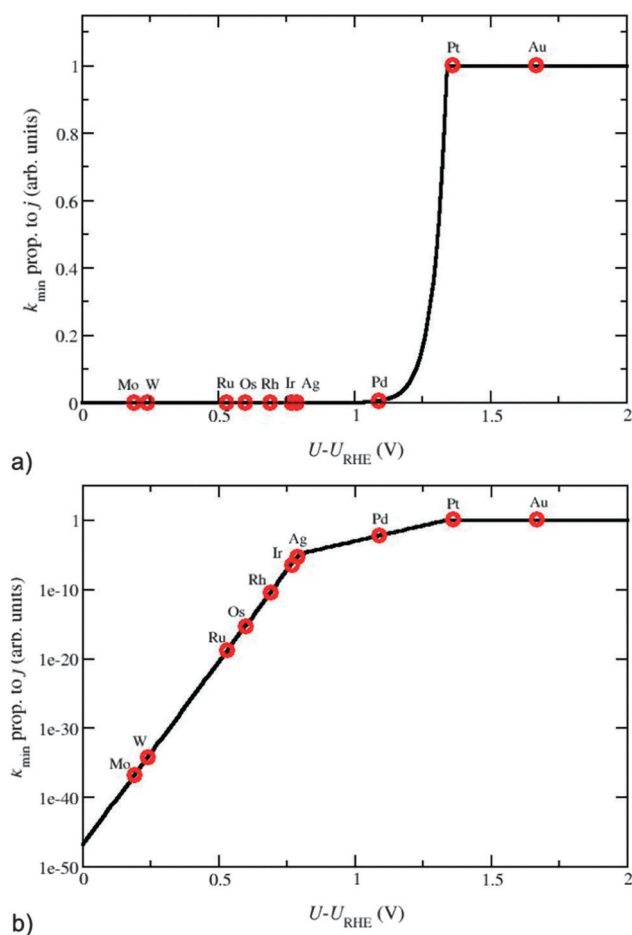


Fig. 7 Normalized maximum SO₂ oxidation rate and the potential at which it is obtained on different transition metals: (a) linear scale and (b) logarithmic scale.

clearly different scaling relations (simply changing to other metal facets or binary alloys is not expected to have enough impact on the scaling relations). An alternative strategy would be to tailor the surface microstructure in a more delicate fashion, forming a mixture of active and inert sites, so as to obtain the right selective properties.³⁷

4. Methods

All calculations were conducted employing the DFT³⁸ code (GPAW ASE)³⁹ with the RPBE⁴⁰ exchange–correlation functional. The reaction free energies of S*, SO₂*, OH*, HSO₃*, O* and SO₃*, under standard conditions and at $U = 0$ V vs. RHE, were calculated on single crystal slabs of Nb, Mo, Ru, Rh, Pd and Ag (4d transition metals), and on Ta, W, Os, Ir, Pt and Au (5d transition metals) according to eqn (5)–(10) with * denoting a free surface or a species adsorbed on the surface:

$$\Delta G_{S^*}^0 = G_{S^*} + 2G_{H_2O(l)} - G_* - 2G_{H_2(g)} - G_{SO_2(g)} \quad (5)$$

$$\Delta G_{SO_2^*}^0 = G_{SO_2^*} - G_* - G_{SO_2(g)} \quad (6)$$

$$\Delta G_{OH^*}^0 = G_{OH^*} + 1/2G_{H_2(g)} - G_* - G_{H_2O(l)} \quad (7)$$

$$\Delta G_{HSO_3^*}^0 = G_{HSO_3^*} + 1/2G_{H_2(g)} - G_* - G_{H_2O(l)} - G_{SO_2(g)} \quad (8)$$

$$\Delta G_{O^*}^0 = G_{O^*} + G_{H_2(g)} - G_* - G_{H_2O(l)} \quad (9)$$

$$\Delta G_{SO_3^*}^0 = G_{SO_3^*} + G_{H_2(g)} - G_* - G_{H_2O(l)} - G_{SO_2(g)} \quad (10)$$

By assuming standard conditions and $U = 0$ V vs. RHE we could use molecular H₂ as a reference energy since H⁺(aq) + e⁻ and 1/2H₂ are in equilibrium under these conditions.⁴¹ Moreover, gas-phase H₂O was used as reference state in eqn (5)–(10). However, the entropy of H₂O was calculated at 0.035 bar, the equilibrium pressure of H₂O at 300 K. The free energy of this reference state is therefore equal to that of liquid water.⁴² The G_{X^*} and $G_{Z(g)}$ in eqn (5)–(10) were calculated according to eqn (11) and (12):

$$G_{X^*} = E_{X^*} + E_{ZPE,X^*} \quad (11)$$

$$G_{Z(g)} = E_{Z(g)} + E_{ZPE,Z(g)} - TS_{Z(g)} \quad (12)$$

where E_{X^*} and $E_{Z(g)}$ are the total electronic energies (as given by DFT) of the surface plus adsorbate X and of the gas phase molecule Z , E_{ZPE,X^*} and $E_{ZPE,Z(g)}$ are the zero-point energies of X^* and $Z(g)$, and $-TS_{Z(g)}$ is the contribution of the gas phase entropy effects to the free energy (room temperature was assumed in all cases).

The thermodynamically stable crystal structures for each metal were considered, *i.e.* hexagonal close-packed (hcp(0001) surface) for Ru and Os, body centred cubic (bcc(110) surface) for Mo, W, Nb and Ta, and face centred cubic (fcc(111) surface) for the rest. The quasi-Newton minimization scheme was employed to relax the ionic degrees of freedom until the maximum force was smaller than 0.05 eV Å⁻¹. All surfaces were

modelled employing a slab that consists of four layers with each layer consisting of 12 atoms (3 × 4). The bottom two layers were fixed with the two top layers, as well as the adsorbates, being allowed to relax. The Kohn–Sham valence states were described on a real-space grid with a spacing of 0.18 Å, and periodic images of the slab were separated by 20 Å of vacuum. The Brillouin zone was sampled employing the Monkhorst–Pack scheme⁴³ with a k -point grid of (4 × 4 × 1) for fcc- and hcp-0001 structures, while a k -point grid of (3 × 3 × 1) was employed for bcc 110 structures.

Acknowledgements

The Catalysis for Sustainable Energy initiative is funded by the Danish Ministry of Science, Technology and Innovation. The generous funding from Anglo American Platinum, the North-West University, as well as support from the Danish Center for Scientific Computing are gratefully acknowledged.

Notes and references

- 1 S. J. Smith, J. van Aardenne, Z. Klimont, R. J. Andres, A. Volke and S. Delgado Arias, *Atmos. Chem. Phys.*, 2011, **11**, 1101.
- 2 European Commission, Joint Research Centre (JRC)/Netherlands Environmental Assessment Agency (PBL), Emission Database for Global Atmospheric Research (EDGAR), release version 4.1, <http://edgar.jrc.ec.europa.eu>, 2010.
- 3 M. Carmo, D. L. Fritz, J. Mergel and D. Stolten, *Int. J. Hydrogen Energy*, 2013, **38**, 4901.
- 4 J. Lee, B. Jeong and J. D. Ocon, *Curr. Appl. Phys.*, 2013, **13**, 309.
- 5 L. E. Brecher and C. K. Wu, *Electrolytic decomposition of water, US Pat.*, 3888750, Westinghouse Electric Corporation, 1975.
- 6 R. J. Kriek, J. P. van Ravenswaay, M. Potgieter, A. Calitz, V. Lates, M. E. Björketun, S. Siahrostami and J. Rossmeisl, *J. South. Afr. Inst. Min. Metall.*, 2013, **113**, 593.
- 7 M. B. Gorenssek, W. A. Summers, C. O. Bolthrunis, E. J. Lahoda, D. T. Allen, R. Greyvenstein, Hybrid Sulfur Process Reference Design and Cost Analysis – Final Report, SRNL-L1200-2008-00002, Rev 1, 12 June, 2009.
- 8 J. A. O'Brien, J. T. Hinkley, S. W. Donne and S.-E. Lindquist, *Electrochim. Acta*, 2010, **55**, 573.
- 9 A. A. Noyes and H. H. Steinour, *J. Am. Chem. Soc.*, 1929, **51**, 1409.
- 10 J. Rossmeisl, Z.-W. Qu, H. Zhu, G.-J. Kroes and J. K. Nørskov, *J. Electroanal. Chem.*, 2007, **607**, 83.
- 11 I. C. Man, H.-Y. Su, F. Calle-Vallejo, H. A. Hansen, J. I. Martinez, N. G. Inoglu, J. Kitchin, T. F. Jaramillo, J. K. Nørskov and J. Rossmeisl, *ChemCatChem*, 2011, **3**, 1159.
- 12 A. C. C. Tseung and S. Jasem, *Electrochim. Acta*, 1977, **22**, 31.
- 13 M. H. Miles, E. A. Klaus, B. P. Gunn, J. R. Locker and W. E. Serafin, *Electrochim. Acta*, 1978, **23**, 521.

- 14 S. Song, H. Zhang, X. Ma, Z. Shao, R. T. Baker and B. Yi, *Int. J. Hydrogen Energy*, 2008, **33**, 4955.
- 15 K. M. Papazisi, A. Siokou, S. Balomenou and D. Tsiplakides, *Int. J. Hydrogen Energy*, 2012, **37**, 16642.
- 16 T. Reier, M. Oezaslan and P. Strasser, *ACS Catal.*, 2012, **2**, 1765.
- 17 V. Petrykin, K. Macounova, O. A. Shlyakhtin and P. Krtil, *Angew. Chem., Int. Ed.*, 2010, **49**, 4813.
- 18 J. Suntivich, K. J. May, H. A. Gasteiger, J. B. Goodenough and Y. Shao-Horn, *Science*, 2011, **334**, 1383.
- 19 S. Trasatti, *Electrochim. Acta*, 1984, **29**, 1503.
- 20 J. Lee and S. H. Langer, *J. Appl. Electrochem.*, 1995, **25**, 353.
- 21 E. T. Seo and D. T. Sawyer, *Electrochim. Acta*, 1965, **10**, 239.
- 22 A. J. Appleby and B. Pinchon, *Int. J. Hydrogen Energy*, 1980, **5**, 253.
- 23 P. W. T. Lu and R. L. Ammon, *J. Electrochem. Soc.*, 1980, **127**, 2610.
- 24 P. W. T. Lu and R. L. Ammon, *Int. J. Hydrogen Energy*, 1982, **7**, 563.
- 25 H. R. Colon-Mercado and D. T. Hobbs, *Electrochem. Commun.*, 2007, **9**, 2649.
- 26 Z. Samec and J. Weber, *Electrochim. Acta*, 1975, **20**, 403.
- 27 T. Wilke, X. Gao, C. G. Takoudis and M. J. Weaver, *J. Catal.*, 1991, **130**, 62.
- 28 C. Quijada and J. L. Vazquez, *Recent Res. Dev. Electrochem.*, 2000, **3**, 137.
- 29 A. J. Appleby and B. Pinchon, *J. Electroanal. Chem.*, 1979, **95**, 59.
- 30 G. Valensi, J. Van Muylder and M. Pourbaix, *Atlas of Electrochemical Equilibria in Aqueous Solutions*, ed. M. Pourbaix, Pergamon Press, Oxford, 1966, vol. 2, p. 545.
- 31 G. Valensi, Technical Report RT. 207 for Centre Belge d'Etude de la Corrosion, 1973, 121.
- 32 F. Abild-Pedersen, J. Greeley, F. Studt, J. Rossmeisl, T. R. Munter, P. G. Moses, E. Skúlason, T. Bligaard and J. K. Nørskov, *Phys. Rev. Lett.*, 2007, **99**, 016105.
- 33 T. Loucka, *J. Electroanal. Chem.*, 1971, **31**, 319.
- 34 J. Rossmeisl, J. K. Nørskov, C. D. Taylor, M. J. Janik and M. Neurock, *J. Phys. Chem. B*, 2006, **110**, 21833.
- 35 J. Greeley, T. F. Jaramillo, J. Bonde, I. Chorkendorff and J. K. Nørskov, *Nat. Mater.*, 2006, **5**, 909.
- 36 M. E. Björketun, A. S. Bondarenko, B. L. Abrams, I. Chorkendorff and J. Rossmeisl, *Phys. Chem. Chem. Phys.*, 2010, **12**, 10536.
- 37 S. Siahrostami, A. Verdager-Casadevall, M. Karamad, D. Deiana, P. Malacrida, B. Wickman, M. Escudero-Escribano, E. A. Paoli, R. Frydendal, T. W. Hansen, I. Chorkendorff, I. Stephens and J. Rossmeisl, *Nat. Mater.*, 2013, **12**, 1137.
- 38 P. Hohenberg and W. Kohn, *Phys. Rev.*, 1964, **136**, B864; W. Kohn and L. J. Sham, *Phys. Rev.*, 1965, **140**, A1133.
- 39 Atomic Simulation Environment, <https://wiki.fysik.dtu.dk/ase>, accessed September 2012 to February 2013; J. J. Mortensen, L. B. Hansen and K. W. Jacobsen, *Phys. Rev. B: Condens. Matter Mater. Phys.*, 2005, **71**, 035109.
- 40 B. Hammer, L. B. Hansen and J. K. Nørskov, *Phys. Rev. B: Condens. Matter Mater. Phys.*, 1999, **59**, 7413.
- 41 J. K. Nørskov, J. Rossmeisl, A. Logadottir, L. Lindqvist, J. R. Kitchin, T. Bligaard and H. Jónsson, *J. Phys. Chem. B*, 2004, **108**, 17886.
- 42 P. W. Atkins, *Physical Chemistry*, Oxford University Press, Oxford, 4th edn, 1992, p. 943.
- 43 H. Monkhorst and D. Pack, *Phys. Rev. B: Solid State*, 1976, **13**, 5186.